



RESEARCH ARTICLE

10.1029/2021JD036081

On the Speciation of Iodine in Marine Aerosol

Juan Carlos Gómez Martín¹ , Alfonso Saiz-Lopez² , Carlos A. Cuevas² , Alex R. Baker³ , and Rafael P. Fernández⁴ 

Key Points:

- Iodide and SOI are more abundant in PM₁, while the coarse fraction is dominated by iodate; iodide is only 30% lower in the coarse fraction
- Iodine speciation in fine aerosol is related to ocean productivity and present a distinct latitudinal variation
- Different chemical regimes correlated with acidic and alkali ions prevail in fine and coarse aerosol speciation

Supporting Information:

Supporting Information may be found in the online version of this article.

Correspondence to:

J. C. Gómez Martín,
jcgoomez@iaa.es

Citation:

Gómez Martín, J. C., Saiz-Lopez, A., Cuevas, C. A., Baker, A. R., & Fernández, R. P. (2022). On the speciation of iodine in marine aerosol. *Journal of Geophysical Research: Atmospheres*, 127, e2021JD036081. <https://doi.org/10.1029/2021JD036081>

Received 21 OCT 2021
Accepted 5 FEB 2022

Author Contributions:

Conceptualization: Juan Carlos Gómez Martín, Alfonso Saiz-Lopez
Data curation: Juan Carlos Gómez Martín, Carlos A. Cuevas, Alex R. Baker
Formal analysis: Juan Carlos Gómez Martín
Funding acquisition: Juan Carlos Gómez Martín, Alfonso Saiz-Lopez
Investigation: Juan Carlos Gómez Martín, Alex R. Baker
Methodology: Juan Carlos Gómez Martín, Alex R. Baker
Resources: Juan Carlos Gómez Martín
Supervision: Juan Carlos Gómez Martín

© 2022 The Authors.

This is an open access article under the terms of the [Creative Commons Attribution-NonCommercial License](https://creativecommons.org/licenses/by/4.0/), which permits use, distribution and reproduction in any medium, provided the original work is properly cited and is not used for commercial purposes.

¹Instituto de Astrofísica de Andalucía, CSIC, Granada, Spain, ²Department of Atmospheric Chemistry and Climate, Institute of Physical Chemistry Rocasolano, CSIC, Madrid, Spain, ³Centre for Ocean and Atmospheric Science, School of Environmental Sciences, University of East Anglia, Norwich, UK, ⁴Institute for Interdisciplinary Science, National Research Council (ICB-CONICET), FCEN-UNCuyo, Mendoza, Argentina

Abstract We have compiled and analyzed a comprehensive data set of field observations of iodine speciation in marine aerosol. The soluble iodine content of fine aerosol (PM₁) is dominated by soluble organic iodine (SOI; ~50%) and iodide (~30%), while the coarse fraction is dominated by iodate (~50%), with nonnegligible amounts of iodide (~20%). The SOI fraction shows an equatorial maximum and minima coinciding with the ocean “deserts,” which suggests a link between soluble iodine speciation in aerosol and ocean productivity. Among the major aerosol ions, organic anions and non-sea-salt sulfate show positive correlations with SOI in PM₁. Alkali cations are positively correlated to iodate and negatively correlated with SOI and iodide in coarse aerosol. These relationships suggest that under acidic conditions iodate is reduced to HOI, which reacts with organic matter to form SOI, a possible source of iodide. In less acidic sea-salt or dust-rich coarse aerosols, HOI oxidation to iodate and reaction with organic matter likely compete.

Plain Language Summary Iodine has a profound impact on tropospheric chemistry and plays a key role in mammalian metabolism. Marine aerosol is an atmospheric iodine reservoir and its carrier to continental food chains. However, the chemistry behind the varying concentrations of iodine-bearing species observed in aerosol is poorly understood, which hinders model predictions about iodine recycling to the gas phase and accumulation in aerosol. To shed some light on this problem, we have compiled and analyzed a global data set of field observations of iodine speciation in aerosol over the ocean between 1983 and 2018. Comparison of the spatial trends of the relative amounts of soluble iodine species in aerosol and ocean surface remote sensing variables reveals a link to ocean productivity, which points to an important role of organics emitted by the ocean and condensed on aerosol surfaces. Furthermore, the speciation of iodine differs between coarse and fine aerosol, which are originated, respectively, from condensation of gases derived from ocean surface emissions (sulfate aerosol) and aeolian processes (sea salt and dust) and, as a consequence of their different composition, have different pH. Overall, organic matter and acidity emerge from our study as the factors controlling iodine speciation in marine aerosol.

1. Introduction

Iodine has a profound impact on tropospheric chemistry through its role in ozone depletion, particle formation, and impact on the oxidative capacity (see Saiz-Lopez et al., 2012, and references therein). In a previous publication (Gómez Martín et al., 2021), we reported the spatial variability of total iodine (TI) in aerosol by compiling and homogenizing a comprehensive data set of field observations at open ocean, insular, and coastal locations and appending to it previously unpublished measurements, spanning a period of 55 years. The analysis of the latitudinal and longitudinal dependence of TI in aerosol provided for the first time observational evidence from the field showing that the dominant global source of atmospheric iodine to the atmosphere is the reaction between iodide and ozone on the sea–water interface (Carpenter et al., 2013). After uptake on particle surfaces, iodine undergoes a rich aqueous-phase chemistry, which is known to depend on the origin and chemical properties of the aerosol (e.g., acidity [Baker & Yodanis, 2021]) but still remains poorly understood. Iodine speciation determines whether recycling to the gas phase can proceed through formation of volatile species, which is thought to occur via iodide (I⁻), or aerosol becomes essentially an atmospheric iodine sink through accumulation of species assumed to be stable and unreactive, that is, iodate (IO₃⁻; Vogt et al., 1999). However, current aerosol chemical schemes cannot explain the concentrations of I⁻, IO₃⁻, and soluble organic iodine (SOI) observed in field campaigns. Models predict negligible concentrations of I⁻ following recycling to the gas phase and high concentrations of IO₃⁻,

Visualization: Juan Carlos Gómez Martín, Carlos A. Cuevas
Writing – original draft: Juan Carlos Gómez Martín

while they do not deal with SOI (Pechtl et al., 2007; Vogt et al., 1999). In contrast, many field observations report highly variable concentrations of I^- , IO_3^- , and SOI in aerosol samples (see e.g., Baker, 2004, 2005; Gäbler & Heumann, 1993; Lai et al., 2008; Wimschneider & Heumann, 1995).

In this study, we adopt the same strategy as in our previous work on TI to shed light on the processes that control the speciation of iodine in aerosol. We have compiled the available iodine speciation data from cruises and coastal and insular ground-based stations with the aim of inspecting the spatial variability of the ensemble and comparing them with other global ocean and aerosol variables. For completeness, we also analyze the size distribution of total and soluble iodine, which were not specifically addressed in our previous work (Gómez Martín et al., 2021). The questions that we want to address in this work are as follows: which species dominates the soluble iodine speciation at different latitudes and longitudes? Where is each species most abundant: in the fine or in the coarse fraction? Can we link the iodine speciation in fine and coarse marine aerosol to other atmospheric and oceanic variables? And is the iodine speciation correlated to the dominant chemical composition of the aerosol substrate?

2. Methods

2.1. Definitions

Aerosol iodine quantities are defined as in Gómez Martín et al. (2021). TI is given by the sum of total soluble iodine (TSI) and nonsoluble iodine (NSI): $TI = TSI + NSI$. TSI encompasses total inorganic iodine ($TII = [I^-] + [IO_3^-]$) and SOI. Note that except for one recent organic speciation work (Yu et al., 2019), the only individual species reported in the majority of field measurement (Tables S1 and S2 in Supporting Information S1) are iodide (I^-) and iodate (IO_3^-). SOI is determined from the TSI, I^- , and IO_3^- observations: $SOI = TSI - [I^-] - [IO_3^-]$. The soluble speciation is the set of three ratios of the concentrations of I^- , IO_3^- , and SOI to TSI.

Iodine in bulk aerosol and in the fine and coarse aerosol fractions are noted respectively as X_{bulk} , X_{fine} , and X_{coarse} ($X = TI, TSI$). Particulate matter with diameter $d < x \mu\text{m}$ is noted as PM_x , and TI and TSI for diameter $d < x \mu\text{m}$ are noted as TI_x and TSI_x . Usually the cutoff between fine and coarse aerosol is established operationally at a particle diameter of 1 μm . This reflects approximately the usual size classification of marine aerosol, characterized by the nuclei ($d < 0.1 \mu\text{m}$), the accumulation mode ($0.1 \mu\text{m} < d < 0.6 \mu\text{m}$), and the coarse mode ($d > 0.6 \mu\text{m}$) (Seinfeld & Pandis, 1998). PM_1 encompasses the nuclei and the accumulation mode and is composed mostly of sulfate aerosol (low pH), while coarse marine aerosol consists of sea-salt aerosol produced by bubble bursting and wave breaking.

2.2. Description and Treatment of Data Sets

In this work, we keep the same campaign labels used in our previous publication on TI (Gómez Martín et al., 2021), for consistency. Tables S1 and S2 in Supporting Information S1 list respectively the 16 cruises (C#) and 12 coastal ground-based (S#) campaigns where aerosol iodine measurements have been carried out. Iodine speciation measurements are heterogeneous and do not always cover the same species or group of species. The data can be classified in five groups according to the iodine species reported and their size segregation in fine and coarse aerosol, as shown in Tables S1 and S2 in Supporting Information S1, and summarized in Table 1. For some of the cruises where the size distribution of soluble iodine species was reported (C4, C6, C10, C14, C17, C19, and C20) there are also measurements of major ion (MI) available (Allan et al., 2009; Baker et al., 2006, 2007; Droste et al., 2021; Martino et al., 2014; Powell et al., 2015), which are used in this work to investigate potential relationships with the iodine observations. MI observations include Na^+ , NH_4^+ , Mg^{2+} , Ca^{2+} , K^+ , Cl^- , NO_3^- , SO_4^{2-} , oxalate ($C_2O_4^{2-}$), Br^- , and methanesulfonate ($CH_3SO_3^-$) and derived quantities such as non-sea-salt (nss) K^+ , Ca^{2+} , and SO_4^{2-} as defined in Baker and Yodanis (2021). Na^+ is the sea-salt tracer. The precursor of $C_2O_4^{2-}$, oxalic acid is emitted from fossil fuel combustion, biomass burning, and biogenic activity, and it is also an oxidation product of both biogenic (isoprene) and of anthropogenic (e.g., cycloalkanes) emissions (Zhou et al., 2015). Combustion of fossil fuel and biomass is a source of NO_3^- , while NH_4^+ is linked to ammonia emissions from agriculture, although it also has background marine sources. The nss ions are tracers of biomass burning, mineral dust, and sulfur emissions (volcanic, biogenic, or anthropogenic), respectively (Martino et al., 2014). $CH_3SO_3^-$

Table 1
Summary of Available Field Observations of Iodine Speciation in Aerosol

Observations	Cruises/stations ^a	Data points	References
TI and TSI in bulk	C5, C7, C11, C12 ^b , C13, S14, S34, S35	167	Gilfedder et al. (2010), Kang et al. (2015), Lai et al. (2008), Sherwen et al. (2016), Xu et al. (2010), Zhang et al. (2016)
TI size distribution	C12 ^b , S1, S2, S4, S9, S20, S28, S31	133	Baker et al. (2000), Barrie et al. (1994), Duce et al. (1965, 1967, 1983), Duce and Woodcock (1971), Jalkanen and Manninen (1996), Liningner et al. (1966)
TSI and speciation size distribution	C4, C6, C10, C12 ^b , C14, C17, C19, C20, part of S32	158	Allan et al. (2009), Baker (2005), Baker and Yodle (2021), Droste (2017), Droste et al. (2021), Gilfedder et al. (2008), Lai (2008), Yodle (2015)
Speciation in fine fraction only	C8, C9, part of S32	74	Gilfedder et al. (2008), Lai et al. (2008, 2011)
Speciation in bulk only	C3, C5, C7, C13, C18, S14, S35	152	Kang et al. (2015), Lai (2008), Tsukada et al. (1987), Wimschneider and Heumann (1995), Xu et al. (2010), Yodle and Baker (2019), Zhang et al. (2016)

^aThe campaign labels are defined in Tables S1 and S2 in Supporting Information S1 and their geographical location is shown in Figure 1. ^bSpeciation measurements for campaign C12 are reported in this work for the first time. The campaign is described in Gómez Martín et al. (2021).

and nss_SO_4^{2-} are oxidation products of marine biogenic DMS (Andreae et al., 1999) but can also be linked to biomass burning, and agricultural and urban emissions.

Some aspects of data treatment are discussed in Text ST1 in Supporting Information S1. Questions related to analytical methods employed to determine iodine speciation, and in particular to potential speciation changes resulting from the use of cellulose filters and ultrasonication due to the formation of oxidants (e.g., H_2O_2 ; Kanthale et al., 2008; Yodle & Baker, 2019), are discussed in Section 4. In this sense, a global comparison of aerosol iodine speciation measurements should help to pinpoint potentially problematic data.

The fraction of TI in aerosol with $d < 1 \mu\text{m}$ and $d > 1 \mu\text{m}$ has only been reported in one campaign (C12). Other campaigns where the fraction of iodine in fine and coarse aerosol was measured report cascade impactor size-segregated data in several size bins (S1, S2, S4, S9, and S31). These data can be binned together for $d < 1 \mu\text{m}$ and $d > 1 \mu\text{m}$ to get the estimates of the distribution of TI between the coarse and fine fraction. Regarding TSI, three campaigns considered a different cutoff radius ($d < 2.5 \mu\text{m}$ in campaigns C8, C9, and part of S32) and only report the soluble speciation for $\text{PM}_{2.5}$.

Figure 1 shows the geographical distributions of the observations of iodine speciation in aerosol. Unfortunately, the speciation data are rather sparse, with an uneven spatial coverage, especially in the longitudinal coordinate. Most measurements were performed in the East and central Atlantic and in the eastern Indian–western Pacific region. Still, the campaigns sampled the complete range of latitudes, which enables a spatial analysis of the data, with the caveat of comparing data obtained at different seasons and years. Because of the uneven special coverage and lack of simultaneity, box and whiskers statistical plots of the speciation are provided. In contrast to TI measurements, long-term series of iodine speciation do not exist. Moreover, the published data are relatively recent, between 1983 and 2018, and most soluble speciation measurements were carried out between 2002 and 2014. This precludes a long-term trend analysis of the speciation data.

Field observations of TI, TSI, iodine enrichment in aerosol and soluble iodine speciation in aerosol in bulk, fine (PM_1 or $\text{PM}_{2.5}$) and coarse aerosol are compiled in the Data Set S1. Field observations of major aerosol ions in fine (PM_1) and coarse aerosol are available in the Data Set S2. In this work, we investigate separately the speciation of iodine in bulk aerosol and in the fine/coarse size fractions. Most of the published fine aerosol data correspond to PM_1 . The PM_1 and $\text{PM}_{2.5}$ data are analyzed independently.

In order to investigate relationships between sea surface variables and the iodine speciation in aerosol, sea surface salinity (SSS), chlorophyll *a* (Chl-*a*), chromophoric dissolved organic matter (CDOM), detritus absorption at 443 nm, and phytoplankton absorption at 443 nm composites have been obtained from the NASA Earth online data open access resources. The SSS composite (25 August 2011 to 7 June 2015) was constructed with data from the Aquarius satellite mission, while the Chl-*a*, CDOM, and 443 nm detritus and phytoplankton absorption composites (4 July 2002 to 20 May 2021) were constructed using MODIS-A satellite data.

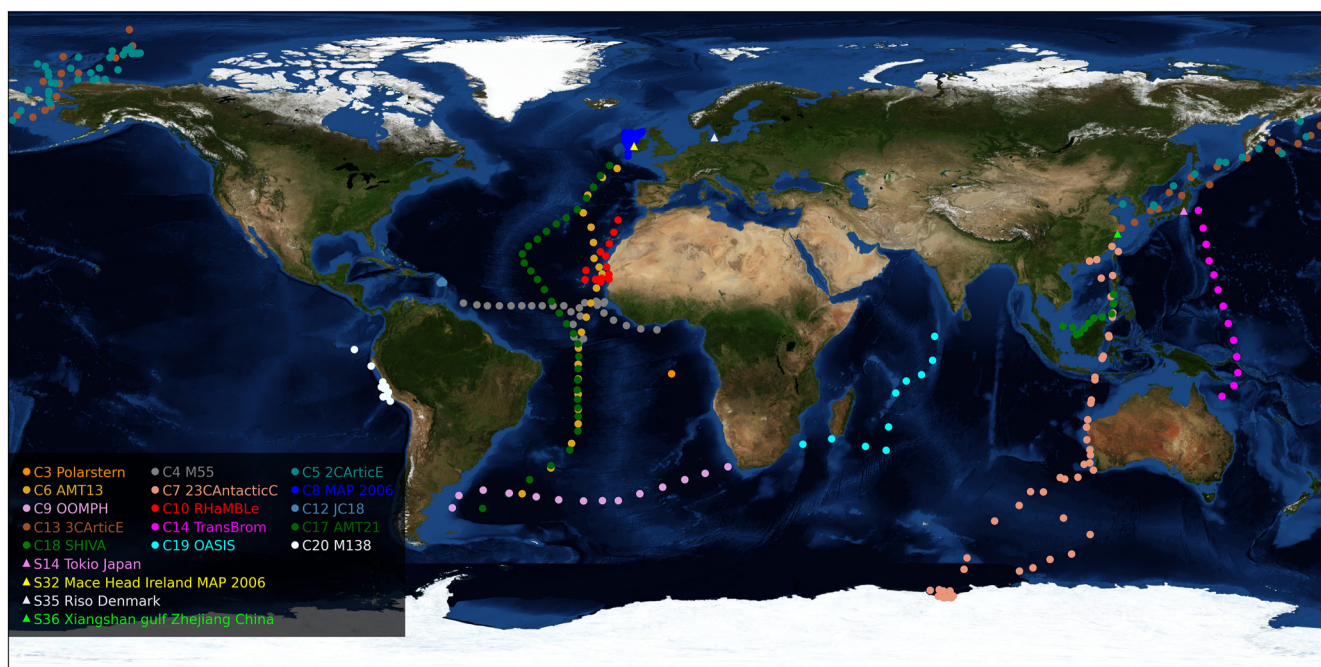


Figure 1. Geographical distribution of soluble iodine speciation observations (measurements of I^- , IO_3^- , and soluble organic iodine [SOI]). Stations: triangles; cruises: dots (see legend). For clarity, campaigns where only the total soluble iodine (TSI)/total iodine (TI) fraction was measured are not included in the map.

3. Results and Discussion

3.1. Size Distribution of TI and TSI

About 40% of iodine (total and soluble) is contained in the PM_{10} aerosol fraction. The content of TI and TSI in the $PM_{2.5}$ fine fraction is higher (~60%), as expected. The latitudinal and longitudinal dependences of the fraction of TI and TSI in fine aerosol for PM_{10} and $PM_{2.5}$ are plotted in Figures S1 and S2 in Supporting Information S1, respectively. No clear spatial trends can be observed. The latitudinal plot suggests higher TI content in the fine aerosol toward the north pole.

3.2. Fraction of Soluble Iodine and Distribution Between Coarse and Fine Aerosol

TSI/TI average, minimum and maximum ratios in bulk aerosol for different campaigns are listed in Table S3 in Supporting Information S1. Figure 2 shows TSI/TI statistics as a function of latitude for 10° zonal bins. These data were already used in our previous publication to scale TSI measurements to TI estimates (Gómez Martín et al., 2021) and therefore will be only briefly discussed. Concurrent TI and TSI observations are available from only eight campaigns (first row in Table 1), while size-segregated measurements of both TI and TSI are only available for campaign C12. In the bulk aerosol, an average of 65%–80% of TI is in soluble form (Figure 2). The average TSI/TI ratio is 66%, while the TSI fraction derived from the slope of a TI versus TSI error-weighted fit is 79% (Gómez Martín et al., 2021). Seven TSI/TI ratios (four in C7 and three in C12) are larger than 1 beyond 2σ analytical uncertainty and have been excluded from the soluble fraction statistical analysis, since $TI = TSI + NSI \geq TSI$ must be fulfilled.

Figure 2 does not show clear latitudinal trends in the bulk TSI/TI ratio. However, lower values were measured in some campaigns at high latitudes (C5, C7, and S35) and higher values in the tropical Atlantic (C12). Figure S3 in Supporting Information S1 shows TSI/TI in bulk aerosol as a function of longitude, for a zonal band between $55^\circ S$ and $55^\circ N$. The campaigns in the Atlantic reporting both TI and TSI show TSI/TI ratios close to 90%–100%, while in the eastern Indian–western Pacific the ratio is closer to ~70%.

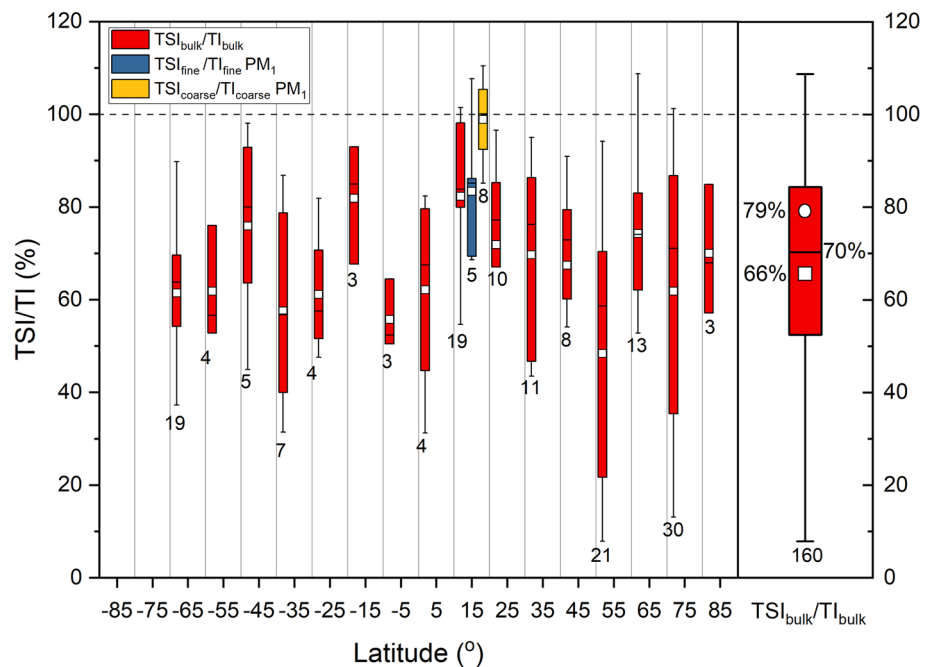


Figure 2. Left panel: latitudinal dependence of the TSI to TI ratio in bulk aerosol (red boxes), in the fine PM₁ fraction (blue), and the coarse fraction (yellow). Right panel: statistics of the TSI/TI ratio in bulk aerosol. The box and whiskers plot statistics are as follows: interquartile range (box), 1.5 × interquartile range (whiskers), median (horizontal line), mean (square), and outliers (diamonds). The circle indicates that the TSI fraction derived from the slope of the TI versus TSI error-weighted linear fit (Gómez Martín et al., 2021). The number of samples is indicated below the boxes.

3.3. Soluble Iodine Speciation: Iodide, Iodate, and SOI

Table S3 in Supporting Information S1 lists descriptive statistics of the bulk iodine speciation ratios measured in the field campaigns included in Tables S1 and S2 in Supporting Information S1. Except for one station at high latitude (S35), the largest contribution to TI is TSI. It can be seen that the contributions of iodide, iodate, and SOI to TSI are highly variable and that in most cases the iodide fraction is nonzero.

Zonal averages in 10° latitude bins of the different X/TSI ratios ($X = \text{SOI}, \text{IO}_3^-, \text{I}^-$) are shown in Figure S4 in Supporting Information S1. There is an increase of SOI toward high latitudes (more pronounced in the Southern Hemisphere, SH), local SOI minima at tropical latitudes, and a local SOI maximum at the equator. Iodide is enhanced toward high latitudes in the Northern Hemisphere (NH). Iodate is enhanced at tropical and equatorial latitudes in both hemispheres, with a possible local minimum at the equator. The global average contributions of SOI, iodate, and iodide to soluble iodine in bulk aerosol are respectively 43%, 29%, and 28% (Figure S4, right panel, in Supporting Information S1). Figure 3a shows 10° zonal averages as Figure S4 in Supporting Information S1 but using a 100% stacked column style, which allows better visualization of these trends. Iodide and SOI show opposite hemispheric gradients in bulk aerosol. Figures 3b and 3c show 100% stacked column plots for soluble iodine species in the fine (PM₁) and coarse fraction, respectively. Trends toward high latitudes cannot be seen in these plots because of the lack of size-segregated speciation measurements beyond 60°N and 50°S. The fine fraction (Figure 3b) is dominated by SOI, which shows a local maximum in the equatorial NH and local minima at 15°S–35°S and 25°N–40°N. I⁻ appears to anticorrelate to SOI, while IO₃⁻ is more or less constant, representing at most 20% of TSI. The coarse fraction (Figure 3c) is dominated by iodate (35%–80%), except in the zonal band centered at 55°N, where almost all soluble iodine is SOI. Such high SOI fraction at this latitude is dominated by the extremely high SOI values measured during the MAP 2006 campaign at Mace Head (S32) and the Irish Sea (C8; note the long ultrasonication times used in the analysis of these samples, see Tables S1 and S2 in Supporting Information S1). The higher IO₃⁻ fraction in coarse aerosol with respect to PM₁ is at the expense of SOI (~20%) and to a lesser extent of iodide (~10%). SOI and IO₃⁻ appear anticorrelated in the coarse fraction, while I⁻ is approximately constant. The local maximum of SOI in the equatorial NH persists in coarse aerosol, concurrent in this case with an IO₃⁻ minimum.

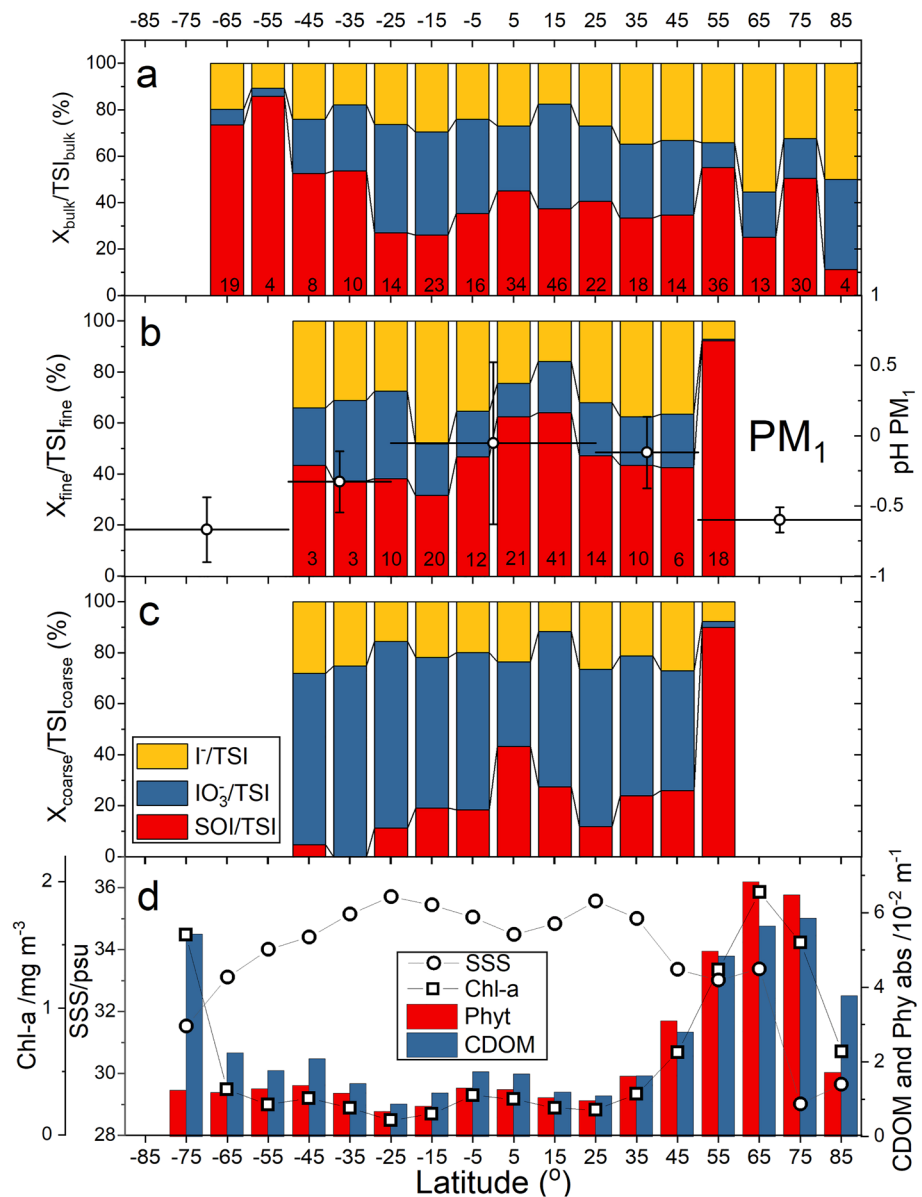


Figure 3. Latitudinal dependence of the TSI speciation. (a) In bulk aerosol, (b) in PM₁, and (c) in coarse aerosol. Red, blue, and yellow stacked columns correspond to SOI, IO₃⁻, and I⁻, respectively. Columns indicate data averages. The number of samples is indicated at the bottom of the columns. The latitudinal averages of PM₁ pH measured in the ATom 1 and 2 campaigns (Nault et al., 2021) are also plotted in (b) (averages: circles, meridional zones: horizontal lines, and spread of measurements: error bars). (d) Sea surface salinity (SSS, circles) from the Aquarius satellite mission, and chlorophyll-*a* concentration (Chl-*a*, squares), CDOM and detritus absorption at 443 nm (CDOM, blue columns), and phytoplankton absorption at 443 nm (Phyt, red columns) from the MODIS-A satellite mission. The satellite averages exclude data for land-locked seas where no measurements of iodine speciation exist (Baltic, Mediterranean, Caspian, Black, and Red Seas and Persian Gulf).

The longitudinal variations of the X/TSI ratios (zonal band 55°S–55°N) are plotted in Figure S5 in Supporting Information S1. The iodide fraction appears to be enhanced in the Pacific, while the iodate fraction is higher at the Atlantic and Indian Oceans. SOI shows a minimum in the eastern Atlantic and western Indian Ocean, which corresponds with regions of lower ocean productivity. For the sake of simplicity, we have not included data for PM_{2.5} in Figure 3 and Figure S5 in Supporting Information S1 (campaigns C8, C9, and part of S32). Analogous latitudinal and longitudinal plots for PM₁ and PM_{2.5} are shown in Figure S6 in Supporting Information S1.

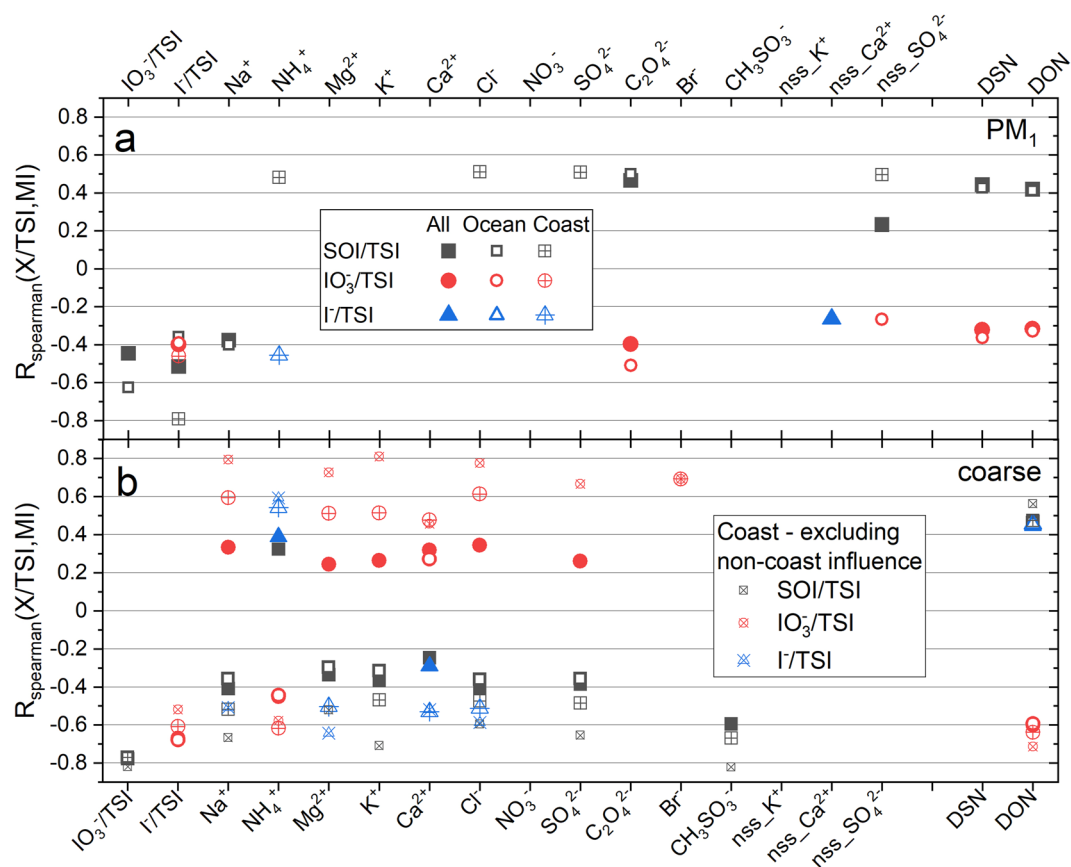


Figure 4. Spearman rank correlation coefficients between major ions in aerosol (MI), pH proxies (degree of sulfate neutralization [DSN] and degree of neutralization [DON]), and the soluble iodine speciation ratios X/TSI for campaigns C4, C6, C10, C14, C17, C19, and C20. Only correlations with $p \leq 0.010$ are shown. (a) Correlation coefficients for PM_{10} aerosol. (b) Correlation coefficients for coarse aerosol. Full, empty, and crossed symbols correspond respectively to the complete data set, open ocean data, and coastal data. (b) Also contains a correlation reanalysis of the coarse coastal data set excluding five datapoints of possible oceanic influence (small crossed symbols).

Campaigns C8 and S32 (North Atlantic) and C9 (southern Atlantic) show an extremely high SOI fraction, with the caveat that all these samples were analyzed with long ultrasonication time (see Section 4).

3.4. Correlation Between Iodine Speciation and MIs

Since $\text{SOI}/\text{TSI} = 1 - \text{TII}/\text{TSI} = 1 - [\text{I}^-]/\text{TSI} - [\text{IO}_3^-]/\text{TSI}$, the SOI fraction is anticorrelated, by definition, with the TII fraction, and is expected to be anticorrelated with at least one of the two components of TII. Figure 4 shows that the SOI fraction is anticorrelated to both the iodide and iodate fractions in PM_{10} but only anticorrelated to iodate in the coarse fraction. The iodate and iodide fractions are anticorrelated both in fine and coarse aerosol, but the anticorrelation is weaker in fine aerosol.

Correlations between MI concentrations in aerosol and iodine speciation ratios have been investigated for the seven cruises (C4, C6, C10, C14, C17, C19, and C20) reporting both types of measurements. This includes a total number of 132 iodine speciation measurements, although in practice each correlation pair may have less data as a result of nondetectable levels of a particular MI species. In addition to investigating correlations for the complete data set (labeled “All” in Figure 4), the data have been divided in two groups: coastal (labeled “Coast”) and open ocean (labeled “Ocean”), based on the distance between the sampling point and the closest continental coast. The idea behind this is highlighting the effect of crustal elements on the iodine speciation. A more rigorous approach would require classification of air masses by origin using back trajectories, which has been done previously for specific cruises (Baker & Yodle, 2021; Yodle & Baker, 2019). The Spearman rank correlation coefficient is used

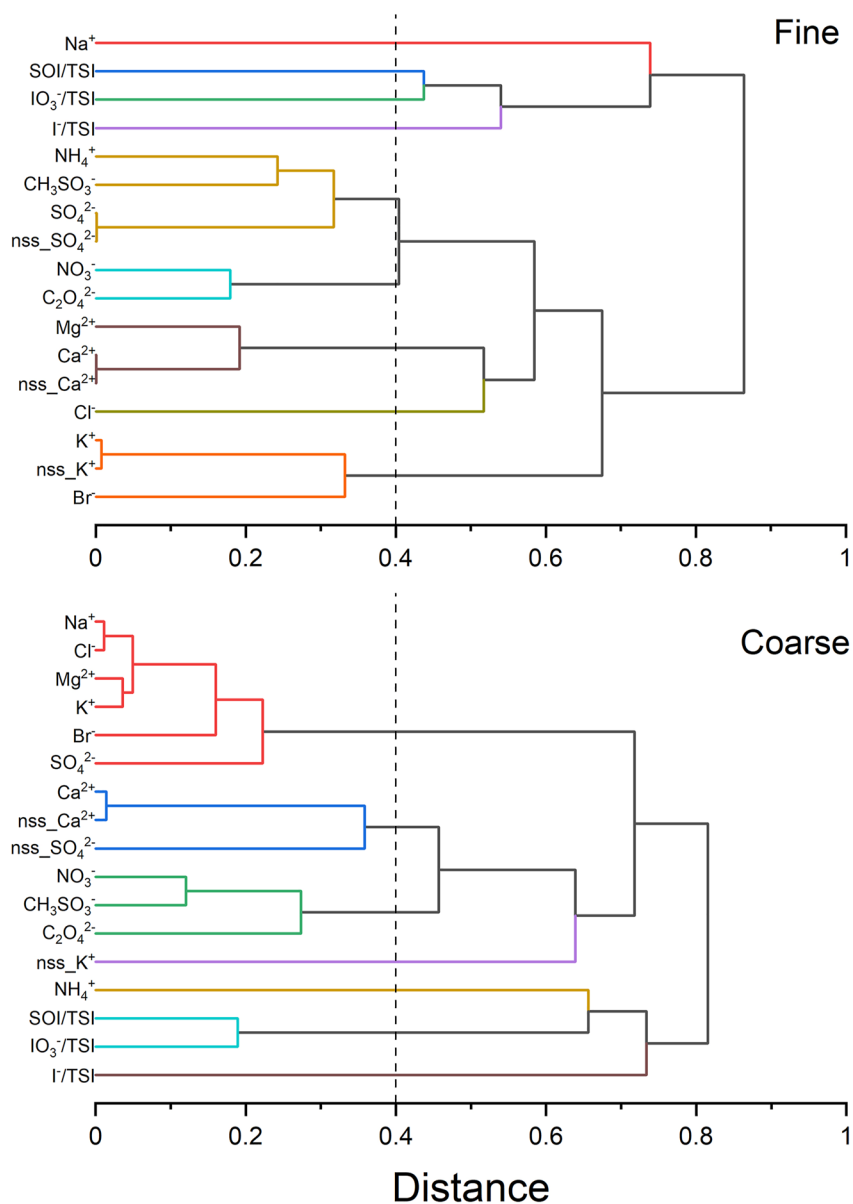


Figure 5. Absolute correlation hierarchical clustering dendrograms (OriginLab, 2020) for iodine speciation and major ion (MI) variables (see Text ST2 in Supporting Information S1). The large data set of aerosol ion observations is reduced by forming affinity groups with a correlation criterion. Top panel: fine (PM₁) aerosol. Bottom panel: coarse aerosol. The vertical dashed line indicates the distance ($R > 0.4$) chosen for the definition of clusters, which are identified by different colors.

instead of the Pearson correlation coefficient, because the relationship between X/TSI ($X = \text{iodide, iodate, SOI}$) and MI is nonlinear due to the nature of the X/TSI ratio (always < 1), as exemplified in Figure 6 for coastal coarse aerosol. Although the Pearson coefficient captures most of the existing correlations, the Spearman rank coefficient is a more robust diagnostic for nonlinear dependences and nonnormally distributed data. Figure 4 shows Spearman correlation coefficients significant at $p = 0.01$ level.

Iodine speciation variables and some MI may be causally linked, but they may also be correlated simply because existing correlations between the different MI resulting from their common sources. Correlation-based hierarchical cluster analysis (Hastie et al., 2009) of the MI data (Text ST2 in Supporting Information S1) indicates five groups or clusters of variables in fine aerosol (Figure 5) that appear both in coastal (Figure S7 in Supporting Information S1) and open ocean data (Figure S8 in Supporting Information S1): the Na⁺ group (sea-salt), the Cl⁻ group (Cl⁻ not linked to sea-salt in fine aerosol), the nss_SO₄²⁻ group (marine biogenic emissions), the

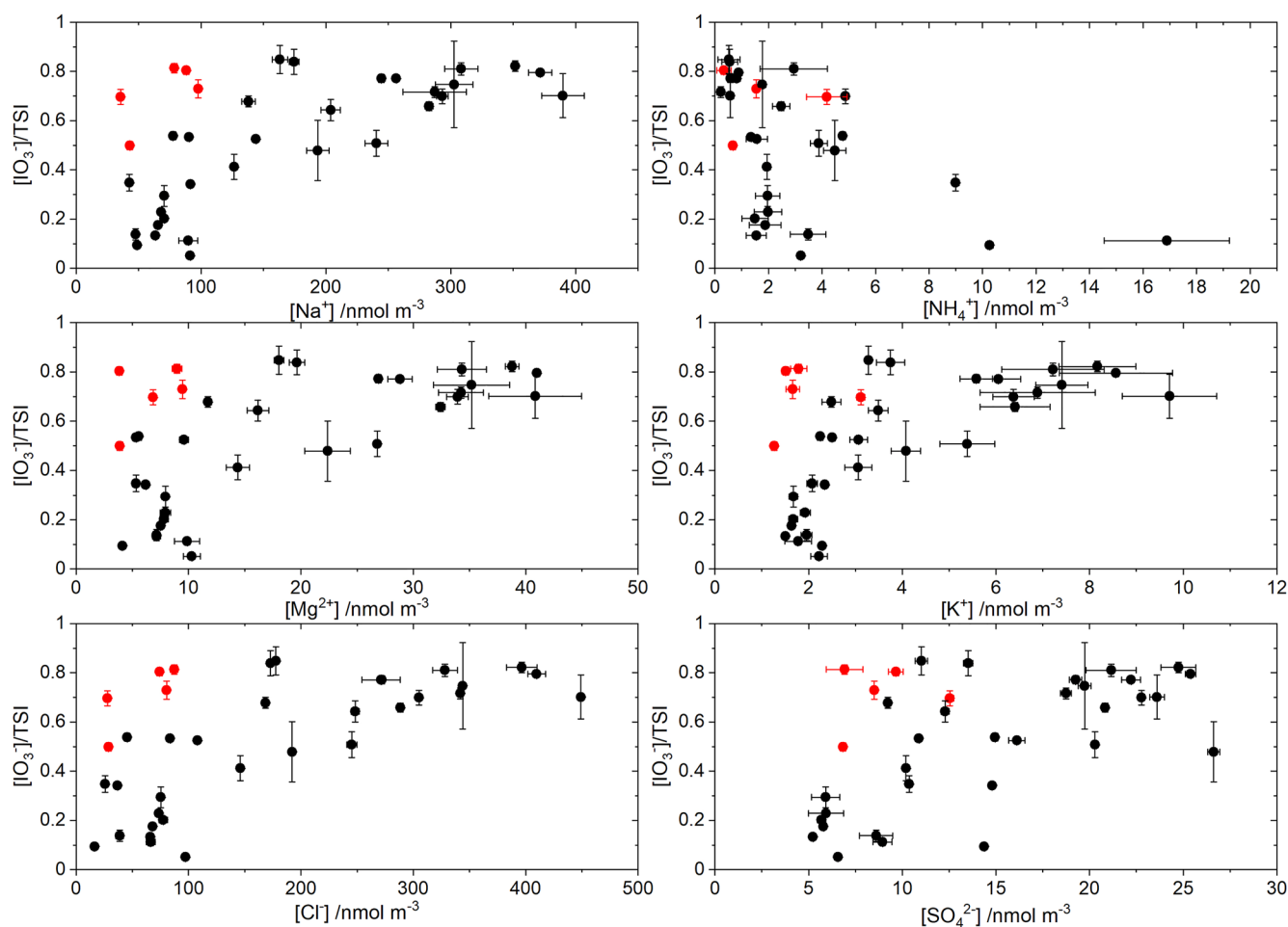


Figure 6. Scatter plots of iodate fraction versus selected MI species for coastal coarse aerosol. The red symbols indicate a group of measurements off the Peruvian ($n = 3$), the East American ($n = 1$), and West African coast ($n = 1$) that appear to deviate from the general trend, possibly because they are not under coastal but under open ocean conditions.

nss_Ca²⁺ group (mineral dust), and the nss_K⁺ group (biomass burning). NO₃⁻, NH₄⁺, CH₃SO₃⁻, and C₂O₄²⁻ appear associated with different groups in the coastal and open ocean subsets. In fine aerosol, most of K⁺, Ca²⁺, and SO₄²⁻ are non-sea-salt ions, that is, nss_X ≈ X, with X = K⁺, Ca²⁺, or SO₄²⁻. Five groups of variables can also be identified for coarse aerosol MI (Figure 5 and Figures S7 and S8 in Supporting Information S1): the sea-salt group (which includes tightly correlated Na⁺, Cl⁻, Mg²⁺, and K⁺, as well as Br⁻ and SO₄²⁻), the mineral dust group (nss_Ca²⁺), the NH₄⁺ group, the NO₃⁻, and C₂O₄²⁻ group (possibly fossil fuel combustion), and the biomass burning group (nss_K⁺). For coarse aerosol Ca²⁺, it is also a non-sea-salt ion (nss_Ca²⁺ ≈ Ca²⁺). The concentration of sea-salt- and dust-related ions is much higher in coarse aerosol (1–2 orders of magnitude).

In fine aerosol, the SOI fraction is positively correlated to some ions within the marine emissions cluster, as well as to Cl⁻ and C₂O₄²⁻, for the coastal data subset. For the open ocean data subset, the SOI fraction is anticorrelated to Na⁺ and positively correlated to C₂O₄²⁻, while the IO₃⁻ fraction is also significantly anticorrelated to C₂O₄²⁻. Note that C₂O₄²⁻ ions are associated with different clusters in the two subsets (Figures S7 and S8 in Supporting Information S1), although both are linked to biomass burning and agricultural emissions (the nitrogen-containing ions cluster for coastal fine aerosol and the nss_K⁺ cluster in the open ocean).

The strongest and more consistent correlations between the iodine speciation variables and MI are for coarse aerosol with the ions classified in the sea-salt, dust, and the NH₄⁺ cluster, and the correlations are stronger for the coastal data. The SOI and I⁻ fractions are anticorrelated to the ions of the Na⁺ and Ca²⁺ clusters, while the IO₃⁻ fraction is positively correlated to the same ions. Conversely, the SOI and I⁻ fractions are positively correlated

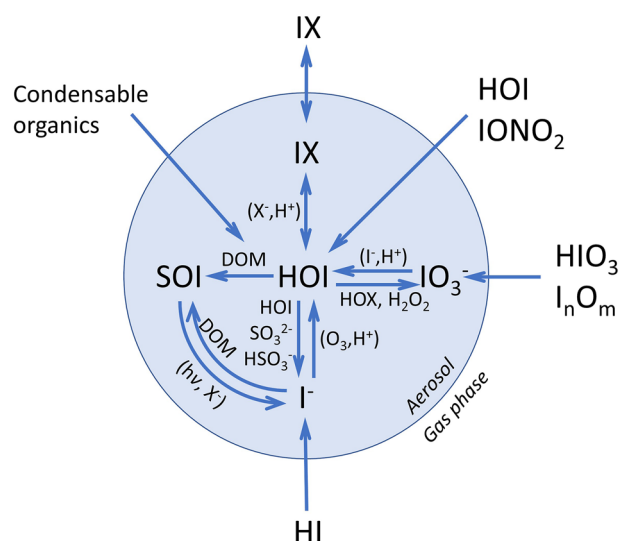


Figure 7. Chemical scheme of soluble iodine in aerosol adapted from Pechtl et al. (2007). The scheme includes SOI explicitly and highlights plausible routes between SOI, I^- , and IO_3^- that may explain the variability observed in the global data set of iodine speciation. Halogen atoms are noted in general as X (X = Cl, Br, I). I_nO_m ($n = 2, m = 2, 3, 4$) denotes iodine oxides. DOM refers to dissolved organic matter. Photolysis is indicated by hv .

to NH_4^+ and the IO_3^- fraction is anticorrelated to NH_4^+ , with the caveat that NH_4^+ concentrations are generally very low in coarse aerosol (Figure 6). Removing a few points of C20 (three points off the West South American coast, latitude $<-15^\circ$ and longitude $<-76^\circ$) and of C4 (one point off the East South American coast, latitude $= 11^\circ$ and longitude $= -59^\circ$, and one point off the West African coast, latitude $= 11^\circ$ and longitude $= -17^\circ$) enhances these correlations (Figure 4b), which is likely a consequence of those data points being under open ocean rather than coastal conditions (Droste et al., 2021). Classification of data by air mass using back trajectory calculations may give higher correlations between iodide species and MI than with the simple coastal/open ocean classification used here (Baker & Yodle, 2021).

Proxies of pH based on aerosol MI observations are based on the cation–anion equivalent ratio or the ion balance method (Pye et al., 2020). In both methods, H^+ is assumed to balance the excess of anions. Two common versions of the cation–anion equivalent ratio are the degree of sulfate neutralization (DSN) and the degree of neutralization (DON). None of these approaches are universal indicators of acidity, since they ignore gas–particle partitioning (Hennigan et al., 2015; Pye et al., 2020). The equivalent ratio in its different flavors may be able to distinguish alkaline particles from acidic particles reliably, although it is unable to quantify aerosol acidity (Hennigan et al., 2015). Figure 4 shows consistent anticorrelation between DON and iodate. Iodide is positively correlated to DON in coarse aerosol.

4. Discussion

On average, 40% of aerosol iodine (total and soluble) exists in PM_1 and about 60% in $PM_{2.5}$. These percentages are consistent along both geographical coordinates. There is some evidence of higher concentration of iodine in fine aerosol at high latitudes, but only from campaign S28 (Barrie et al., 1994). The fraction of TSI in TI is also consistent across latitude and longitude ($\sim 65\%$ – 80%). There is only one campaign at low latitudes (C12 [Gómez Martín et al., 2021]), reporting almost all TI being soluble, while another campaign (S35 [Zhang et al., 2016]) reports an extremely high nonsoluble fraction (82%), with complete absence of iodate and SOI. Insoluble aerosol iodine does not seem to be linked to coastal new particle formation as previously speculated (Baker, 2004), since it appears to exist ubiquitously, and iodine-driven new particle formation leads to iodic acid particles (Gómez Martín et al., 2020) and ultimately to iodate. The campaign reporting dominant NSI took place in a coastal location, but not in open ocean waters, and with some influence of continental air (Risø, Denmark, S35). Recent work has demonstrated the presence of abundant NSI compounds in a continental location related to anthropogenic activities (Shi et al., 2021).

Iodine is enriched in aerosol compared to seawater, as a result of the uptake of gas-phase iodine compounds (Duce et al., 1983). As schematically depicted in Figure 7, the uptake of HI, HOI, $IONO_2$ leads to the formation of I^- , while uptake of iodine oxides is expected to form IO_3^- . Part of SOI present in seawater may be incorporated into aerosol from bubble bursting (primary SOI), but the fine mode dominance of SOI suggests that a larger fraction forms after sorption of gas-phase iodine into particles (secondary SOI). It has been previously suggested that dissolved organic matter (DOM) in aerosol reacts with HOI to form SOI (Baker, 2005). Photolysis of SOI can potentially form I^- , as has been observed for alkyl halides (Jones & Carpenter, 2005; Martino et al., 2005). Organic compounds and iodide could also form adducts (i.e., SOI) as reported by Yu et al. (2019), leading to SOI–iodide interconversion, although the use of long ultrasonication times and cellulose filters makes the organic speciation reported in that work somewhat uncertain (Yodle & Baker, 2019).

The higher fractions of SOI and I^- in fine aerosol (respectively $\sim 50\%$ and $\sim 30\%$ on average for the complete data set) and higher fraction of iodate in coarse aerosol ($\sim 50\%$) but with nonnegligible iodide ($\sim 20\%$) have been previously documented for individual cruise data sets (Baker, 2004, 2005; Baker & Yodle, 2021; Droste et al., 2021). Figure 3 indicates that SOI, both in coarse and fine aerosol, has an equatorial maximum, minima in the tropical “desert ocean” region, and again enhanced values at middle-high latitudes. This latitudinal distribution is

reminiscent of the average latitudinal profiles of Chl-*a*, phytoplankton absorption at 443 nm and CDOM and detritus absorption at 443 nm measured by MODIS-A (see Figure 3d), suggesting that organic compounds derived from oceanic emissions or incorporated in bubble bursting may exert some control on the SOI and I^- fractions. Some MI tracers of biogenic emissions are correlated to the iodine speciation in PM_{10} , suggesting that SOI forms from reactions between organics that have condensed on sulfate aerosol, forming DOM, and an iodine-containing species (HOI or I^-). The SOI and IO_3^- fractions in PM_{10} are respectively correlated and anticorrelated to oxalate, $C_2O_4^{2-}$. Oxalate grows toward the NH, as can be expected from its partly anthropogenic sources, but the latitudinal profile shows some evidence of a superposed biogenic oceanic source (local equatorial maximum and tropical minima, Figure S9c in Supporting Information S1). However, SOI is also anticorrelated to the sea-salt tracer Na^+ (which itself tracks SSS), which may indicate that there is less organic matter incorporated into aerosol by bubble bursting in the high SSS ocean “deserts.”

The larger fraction of IO_3^- in coarse aerosol, with a nonnegligible fraction of I^- (Figure 3), and the anticorrelation between the I^- and IO_3^- fractions both in fine and coarse aerosol (Figure 4) indicate that iodate is not a permanent iodine sink. The Dushman reaction and the Bray–Liebhafsky mechanism have been previously invoked to explain qualitatively the reduction of iodate to iodide under different acidity conditions (Koenig et al., 2020; Pechtl et al., 2007). I_2 formed from iodate reduction would be in equilibrium with HOI, which would react with DOM leading to the formation of SOI. Also, under acidic conditions, I^- could possibly be oxidized faster to HOI (Figure 7), explaining anticorrelation between SOI and I^- in PM_{10} , but not in coarse aerosol (Figure 4). Sulfate aerosol is acidic (Pye et al., 2020), with pH generally between 1 and 3, that can also take negative values, as shown by the boundary layer pH data for PM_{10} in Figure 3b (ATom campaigns [Nault et al., 2021]). Freshly emitted coarse sea-salt aerosol maintains its high pH for a very short period and then acidifies to values around 4–5 (Angle et al., 2021), and dust aerosol is basic in nature (Pye et al., 2020). The campaigns reporting iodine speciation and MI do not include concurrent measurements or estimates of pH. Observations of aerosol pH are only available for a limited number of field campaigns. Nevertheless, the correlations with MI species in Figure 4 are informative about potential links between acidity and the iodine speciation. The positive correlation between the iodate fraction and alkali cations (coincident with a negative correlation for the SOI and iodide fractions) suggests a role of acidity in iodate reduction, since more alkaline ions would mean less acidic sea-salt or dust aerosol and accumulation of iodate (Baker & Yodle, 2021; Droste et al., 2021). Coarse aerosol collected close to the coast shows 1 order of magnitude higher content of crustal ions, which explains the enhanced correlations in Figure 4b. By contrast, Figure 4a shows a positive correlation in acidic PM_{10} between SOI and $nss_SO_4^{2-}$. The pH proxies DSN and DON are anticorrelated to iodate and positively correlated to SOI, which supports the role of acidity in controlling the IO_3^- fraction. Hence, we suggest that the latitudinal variation of iodate and SOI in coarse aerosol (Figure S10 in Supporting Information S1) is mainly controlled by acidity, in contrast to fine aerosol, where the latitudinal variation of iodide and SOI appears to be controlled by organics (Figure S9 in Supporting Information S1).

Xu et al. (2010) and Yodle and Baker (2019) assessed the optimal analytical methodology for full iodine recovery and speciation stability. Both studies confirmed earlier evidence that extended periods of ultrasonication leads to changes in iodine speciation (formation of SOI; Baker et al., 2000), especially when cellulose filters are used. Ultrasonication power and frequency are significant factors in the generation of hydrogen peroxide that is thought to be responsible for iodine speciation change (Kanthale et al., 2008; Saiz-Lopez et al., 2012), but these parameters are rarely reported in iodine speciation studies. Recent results indicate that SOI formation during ultrasonication is dependent on the inorganic iodine speciation of the aerosol sample (Yu et al., 2019). Hence, long ultrasonication times with cellulose substrates are currently not recommended and the impacts of this procedure within and between affected data sets are likely to be variable, depending on the equipment used and the composition of the samples themselves.

Within the available bulk aerosol data, 78 out of 311 samples (C7, S32, and S36) used very long sonication times (20 min and longer). Of those studies, only some of the C7 samples were geographically located in a similar region to a study in which ultrasonication was not used (C18 [Yodle & Baker, 2019]). The range of TSI concentrations reported for the C18 samples was similar to the range reported for C7 in samples in coastal waters of southeast Asia (Lai et al., 2008). SOI dominated (>60%) the speciation of the C7 samples, with IO_3^- contributing less than 10% to TSI, whereas during C18 iodate and iodide were the dominant species (~40% [median] of TSI

each). For PM₁/coarse aerosol, 18 out of 158 samples (all belonging to S32) were obtained with long ultrasonication. For PM_{2.5}, all samples were analyzed with long ultrasonication time (C8 and C9).

Assuming that the analytical methods, and not natural variability, are the cause of the differences in iodine speciation between the C7 and C18 data sets, introduces the possibility of a methodological bias in the global data set. We have examined the impact of this potential bias on our conclusions by excluding the C7, S32, and S36 campaigns from the analysis of latitudinal speciation trends in bulk and PM₁/coarse aerosol (see Figure S11 in Supporting Information S1). While the excluded data do appear to exhibit higher proportions of SOI than the rest of the data set (and all the available PM_{2.5} data, see Figure S6 in Supporting Information S1), the overall latitudinal variation in iodine speciation in bulk and PM₁/coarse aerosol is very similar (Figure 3 and Figure S11 in Supporting Information S1). The longitudinal variability (Figure S5 in Supporting Information S1) may be more compromised by analytical biases, since most cruises are latitudinal transects. Nevertheless, there is currently insufficient evidence to draw firm conclusions on whether iodine speciation was altered during analysis in campaigns C7, C8, C9, S32, and S36, or whether the observed speciation differences are the result of natural variability.

5. Conclusions

There are some uncertainties regarding the different analytical methods employed in the determination of iodine speciation in aerosol, and we recommend that future work considers carefully the problems associated with the combination of cellulose filters and long time (and/or high power) ultrasonic extraction. However, the correspondence between the spatial trends of ocean productivity variables and the SOI fraction in marine aerosol determined from the global iodine speciation data set compiled in this work, and the correlations between iodine speciation ratios and MI concurrently measured in seven cruises indicate that the two acidity regimes and the availability of organics are major controlling factors of the iodide–iodate–SOI variability, as summarized in the chemical scheme in Figure 7. Future laboratory and modeling work needs to address the underlying chemical and photochemical reactions of this system, especially regarding the reactions between DOM and HOI and the photochemical processes linking SOI and iodide.

Conflict of Interest

The authors declare no conflicts of interest relevant to this study.

Data Availability Statement

MODIS-A Level 3 data products (chlorophyll-*a*, CDOM, and detritus absorption at 443 nm and phytoplankton absorption at 443 nm) can be downloaded from NASA's Ocean Color Web (<https://oceancolor.gsfc.nasa.gov/>). SSS data from the Aquarius satellite mission can be downloaded from NASA's Physic Oceanography Distributed Active Archive Center (<http://podaac.jpl.nasa.gov/SeaSurfaceSalinity/Aquarius>). Total iodine, total soluble iodine, iodine enrichment factors, iodine speciation, and major ion aerosol observations in marine aerosol compiled for this work can be retrieved from <https://doi.org/10.5281/zenodo.5588450>.

Acknowledgments

The authors are grateful to Zhouqing Xie, Senchao Lai, and Benjamin Gilfedder for assisting in the retrieval of historical data. J. C. G. M. acknowledges financial support from the State Agency for Research of the Spanish MCIU through the "Center of Excellence Severo Ochoa" award to the Instituto de Astrofísica de Andalucía (SEV-2017-0709) and the Ramon y Cajal Program (RYC-2016-19570). A. S.-L. acknowledges financial support from the European Research Council Executive Agency under the European Union's Horizon 2020 Research and Innovation program (Project "ERC-2016-COG 726349 CLIMAHAL").

References

- Allan, J. D., Topping, D. O., Good, N., Irwin, M., Flynn, M., Williams, P. I., et al. (2009). Composition and properties of atmospheric particles in the eastern Atlantic and impacts on gas phase uptake rates. *Atmospheric Chemistry and Physics*, 9(23), 9299–9314. <https://doi.org/10.5194/acp-9-9299-2009>
- Andreae, M. O., Elbert, W., Cai, Y., Andreae, T. W., & Gras, J. (1999). Non-sea-salt sulfate, methanesulfonate, and nitrate aerosol concentrations and size distributions at Cape Grim, Tasmania. *Journal of Geophysical Research*, 104(D17), 21695–21706. <https://doi.org/10.1029/1999JD900283>
- Angle, K. J., Crocker, D. R., Simpson, R. M. C., Mayer, K. J., Garofalo, L. A., Moore, A. N., et al. (2021). Acidity across the interface from the ocean surface to sea spray aerosol. *Proceedings of the National Academy of Sciences of the United States of America*, 118(2), e2018397118. <https://doi.org/10.1073/pnas.2018397118>
- Baker, A. R. (2004). Inorganic iodine speciation in tropical Atlantic aerosol. *Geophysical Research Letters*, 31, L23S02. <https://doi.org/10.1029/2004GL020144>
- Baker, A. R. (2005). Marine aerosol iodine chemistry: The importance of soluble organic iodine. *Environmental Chemistry*, 2(4), 295–298. <https://doi.org/10.1071/EN05070>

- Baker, A. R., Jickells, T. D., Biswas, K. F., Weston, K., & French, M. (2006). Nutrients in atmospheric aerosol particles along the Atlantic Meridional Transect. *Deep-Sea Research Part II: Topical Studies in Oceanography*, 53(14–16), 1706–1719. <https://doi.org/10.1016/j.dsr2.2006.05.012>
- Baker, A. R., Thompson, D., Campos, M. L. A. M., Parry, S. J., & Jickells, T. D. (2000). Iodine concentration and availability in atmospheric aerosol. *Atmospheric Environment*, 34(25), 4331–4336. [https://doi.org/10.1016/S1352-2310\(00\)00208-9](https://doi.org/10.1016/S1352-2310(00)00208-9)
- Baker, A. R., Weston, K., Kelly, S. D., Voss, M., Streu, P., & Cape, J. N. (2007). Dry and wet deposition of nutrients from the tropical Atlantic atmosphere: Links to primary productivity and nitrogen fixation. *Deep-Sea Research Part I: Oceanographic Research Papers*, 54(10), 1704–1720. <https://doi.org/10.1016/j.dsr.2007.07.001>
- Baker, A. R., & Yodle, C. (2021). Indirect evidence for the controlling influence of acidity on the speciation of iodine in Atlantic aerosols. *Atmospheric Chemistry and Physics*, 21(17), 13067–13076. <https://doi.org/10.5194/ACP-21-13067-2021>
- Barrie, L. A., Staebler, R., Toom, D., Georgi, B., den Hartog, G., Landsberger, S., & Wu, D. (1994). Arctic aerosol size-segregated chemical observations in relation to ozone depletion during Polar Sunrise Experiment 1992. *Journal of Geophysical Research*, 99(D12), 25439–25451. <https://doi.org/10.1029/94JD01514>
- Carpenter, L. J., MacDonald, S. M., Shaw, M. D., Kumar, R., Saunders, R. W., Parthipan, R., et al. (2013). Atmospheric iodine levels influenced by sea surface emissions of inorganic iodine. *Nature Geoscience*, 6(2), 108–111. <https://doi.org/10.1038/ngeo1687>
- Droste, E. S. (2017). *Soluble iodine speciation in Indian Ocean aerosols and its impact on marine boundary layer chemistry* (Master's thesis). Norwich, UK/Wageningen, The Netherlands: University of East Anglia/Wageningen University & Research.
- Droste, E. S., Baker, A. R., Yodle, C., Smith, A., & Ganzeveld, L. (2021). Soluble iodine speciation in marine aerosols across the Indian and Pacific Ocean Basins. *Frontiers in Marine Science*, 8, 788105. <https://doi.org/10.3389/FMARS.2021.788105>
- Duce, R. A., Arimoto, R., Ray, B. J., Unni, C. K., & Harder, P. J. (1983). Atmospheric trace elements at Enewetak Atoll: 1. Concentrations, sources, and temporal variability. *Journal of Geophysical Research*, 88(C9), 5321–5342. <https://doi.org/10.1029/JC088iC09p05321>
- Duce, R. A., Winchester, J. W., & Van Nahl, T. W. (1965). Iodine, bromine, and chlorine in the Hawaiian marine atmosphere. *Journal of Geophysical Research*, 70(8), 1775–1799. <https://doi.org/10.1029/JZ070i008p01775>
- Duce, R. A., & Woodcock, A. H. (1971). Difference in chemical composition of atmospheric sea salt particles produced in the surf zone and on the open sea in Hawaii. *Tellus*, 23(4–5), 427–435. <https://doi.org/10.3402/tellusa.v23i4-5.10520>
- Duce, R. A., Woodcock, A. H., & Moyers, J. L. (1967). Variation of ion ratios with size among particles in tropical oceanic air. *Tellus*, 19(3), 369–379. <https://doi.org/10.1111/j.2153-3490.1967.tb01492.x>
- Gäbler, H.-E., & Heumann, K. G. (1993). Determination of atmospheric iodine species using a system of specifically prepared filters and IDMS. *Fresenius' Journal of Analytical Chemistry*, 345(1), 53–59. <https://doi.org/10.1007/bf00323326>
- Gilfedder, B. S., Chance, R. J., Dettmann, U., Lai, S. C., & Baker, A. R. (2010). Determination of total and non-water soluble iodine in atmospheric aerosols by thermal extraction and spectrometric detection (TESD). *Analytical and Bioanalytical Chemistry*, 398(1), 519–526. <https://doi.org/10.1007/s00216-010-3923-1>
- Gilfedder, B. S., Lai, S. C., Petri, M., Biester, H., & Hoffmann, T. (2008). Iodine speciation in rain, snow and aerosols. *Atmospheric Chemistry and Physics*, 8(20), 6069–6084. <https://doi.org/10.5194/acp-8-6069-2008>
- Gómez Martín, J. C., Lewis, T. R., Blitz, M. A., Plane, J. M. C., Kumar, M., Francisco, J. S., & Saiz-Lopez, A. (2020). A gas-to-particle conversion mechanism helps to explain atmospheric particle formation through clustering of iodine oxides. *Nature Communications*, 11(1), 1–14. <https://doi.org/10.1038/s41467-020-18252-8>
- Gómez Martín, J. C., Saiz-Lopez, A., Cuevas, C. A., Fernandez, R. P., Gilfedder, B., Weller, R., et al. (2021). Spatial and temporal variability of iodine in aerosol. *Journal of Geophysical Research: Atmospheres*, 126, e2020JD034410. <https://doi.org/10.1029/2020JD034410>
- Hastie, T., Tibshirani, R., & Friedman, J. (2009). *The elements of statistical learning*. New York: Springer. <https://doi.org/10.1007/978-0-387-84858-7>
- Hennigan, C. J., Izumi, J., Sullivan, A. P., Weber, R. J., & Nenes, A. (2015). A critical evaluation of proxy methods used to estimate the acidity of atmospheric particles. *Atmospheric Chemistry and Physics*, 15(5), 2775–2790. <https://doi.org/10.5194/acp-15-2775-2015>
- Jalkanen, L., & Manninen, P. (1996). Multivariate data analysis of aerosols collected on the Gulf of Finland. *Environmetrics*, 7(1), 27–38. [https://doi.org/10.1002/\(SICI\)1099-095x\(199601\)7:1<27::AID-ENV159>3.0.CO;2-3](https://doi.org/10.1002/(SICI)1099-095x(199601)7:1<27::AID-ENV159>3.0.CO;2-3)
- Jones, C. E., & Carpenter, L. J. (2005). Solar photolysis of CH₂I₂, CH₂ICl, and CH₂I₂Br in water, saltwater, and seawater. *Environmental Science and Technology*, 39(16), 6130–6137. <https://doi.org/10.1021/es050563g>
- Kang, H., Xu, S., Yu, X., Li, B., Liu, W., Yang, H., & Xie, Z. (2015). Iodine speciation in aerosol particle samples collected over the sea between offshore China and the Arctic Ocean. *Advances in Polar Science*, 26(3), 215–221. <https://doi.org/10.13679/j.advps.2015.3.00215>
- Kanthale, P., Ashokkumar, M., & Grieser, F. (2008). Sonoluminescence, sonochemistry (H₂O₂ yield) and bubble dynamics: Frequency and power effects. *Ultrasonics Sonochemistry*, 15(2), 143–150. <https://doi.org/10.1016/j.ultsonch.2007.03.003>
- Koenig, T. K., Baidar, S., Campuzano-Jost, P., Cuevas, C. A., Dix, B., Fernandez, R. P., et al. (2020). Quantitative detection of iodine in the stratosphere. *Proceedings of the National Academy of Sciences of the United States of America*, 117(4), 1860–1866. <https://doi.org/10.1073/PNAS.1916828117>
- Lai, S. C. (2008). *Iodine speciation in atmospheric aerosols in the marine boundary layer* (Doctoral dissertation). Mainz, Germany: Johannes Gutenberg-Universität Mainz.
- Lai, S. C., Hoffmann, T., & Xie, Z. Q. (2008). Iodine speciation in marine aerosols along a 30,000 km round-trip cruise path from Shanghai, China to Prydz Bay, Antarctica. *Geophysical Research Letters*, 35, L21803. <https://doi.org/10.1029/2008GL035492>
- Lai, S. C., Williams, J., Arnold, S. R., Atlas, E. L., Gebhardt, S., & Hoffmann, T. (2011). Iodine containing species in the remote marine boundary layer: A link to oceanic phytoplankton. *Geophysical Research Letters*, 38, L20801. <https://doi.org/10.1029/2011GL049035>
- Lininger, R. L., Duce, R. A., Winchester, J. W., & Matson, W. R. (1966). Chlorine, bromine, iodine, and lead in aerosols from Cambridge, Massachusetts. *Journal of Geophysical Research*, 71(10), 2457–2463. <https://doi.org/10.1029/JZ071i010p02457>
- Martino, M., Hamilton, D., Baker, A. R., Jickells, T. D., Bromley, T., Nojiri, Y., et al. (2014). Western Pacific atmospheric nutrient deposition fluxes, their impact on surface ocean productivity. *Global Biogeochemical Cycles*, 28, 712–728. <https://doi.org/10.1002/2013GB004794>
- Martino, M., Liss, P. S., & Plane, J. M. C. (2005). The photolysis of dihalomethanes in surface seawater. *Environmental Science and Technology*, 39(18), 7097–7101. <https://doi.org/10.1021/es048718s>
- Nault, B. A., Campuzano-Jost, P., Day, D. A., Jo, D. S., Schroder, J. C., Allen, H. M., et al. (2021). Chemical transport models often underestimate inorganic aerosol acidity in remote regions of the atmosphere. *Communications Earth & Environment*, 2(1), 93. <https://doi.org/10.1038/s43247-021-00164-0>
- OriginLab. (2020). *Online help: 17.7.3.3 Algorithms (Hierarchical Cluster Analysis)*. Retrieved from <https://www.originlab.com/doc/Origin-Help/HCA-Algorithm>
- Pechtl, S., Schmitz, G., & von Glasow, R. (2007). Modelling iodide–iodate speciation in atmospheric aerosol: Contributions of inorganic and organic iodine chemistry. *Atmospheric Chemistry and Physics*, 7(5), 1381–1393. <https://doi.org/10.5194/acp-7-1381-2007>

- Powell, C. F., Baker, A. R., Jickells, T. D., Bange, H. W., Chance, R. J., & Yodle, C. (2015). Estimation of the atmospheric flux of nutrients and trace metals to the eastern tropical North Atlantic Ocean. *Journal of the Atmospheric Sciences*, 72(10), 4029–4045. <https://doi.org/10.1175/JAS-D-15-0011.1>
- Pye, H. O. T., Nenes, A., Alexander, B., Ault, A. P., Barth, M. C., Clegg, S. L., et al. (2020). The acidity of atmospheric particles and clouds. *Atmospheric Chemistry and Physics*, 20, 4809–4888. <https://doi.org/10.5194/acp-20-4809-2020>
- Saiz-Lopez, A., Plane, J. M. C., Baker, A. R., Carpenter, L. J., von Glasow, R., Gómez Martín, J. C., et al. (2012). Atmospheric chemistry of iodine. *Chemical Reviews*, 112(3), 1773–1804. <https://doi.org/10.1021/cr200029u>
- Seinfeld, J. H., & Pandis, S. N. (1998). *Atmospheric chemistry and physics*. New York: Wiley-Interscience.
- Sherwen, T. M., Evans, M. J., Spracklen, D. V., Carpenter, L. J., Chance, R., Baker, A. R., et al. (2016). Global modeling of tropospheric iodine aerosol. *Geophysical Research Letters*, 43, 10012–10019. <https://doi.org/10.1002/2016GL070062>
- Shi, X., Qiu, X., Chen, Q., Chen, S., Hu, M., Rudich, Y., & Zhu, T. (2021). Organic iodine compounds in fine particulate matter from a continental urban region: Insights into secondary formation in the atmosphere. *Environmental Science and Technology*, 55(3), 1508–1514. <https://doi.org/10.1021/acs.est.0c06703>
- Tsukada, H., Hara, H., Iwashima, K., & Yamagata, N. (1987). The iodine content of atmospheric aerosols as determined by the use of a Fluoropore Filter® for collection. *Bulletin of the Chemical Society of Japan*, 60(9), 3195–3198. <https://doi.org/10.1246/bcsj.60.3195>
- Vogt, R., Sander, R., Von Glasow, R., & Crutzen, P. J. (1999). Iodine chemistry and its role in halogen activation and ozone loss in the marine boundary layer: A model study. *Journal of Atmospheric Chemistry*, 32(3), 375–395. <https://doi.org/10.1023/a:1006179901037>
- Wimschneider, A., & Heumann, K. G. (1995). Iodine speciation in size fractionated atmospheric particles by isotope dilution mass spectrometry. *Fresenius' Journal of Analytical Chemistry*, 353(2), 191–196. <https://doi.org/10.1007/bf00322957>
- Xu, S., Xie, Z., Li, B., Liu, W., Sun, L., Kang, H., et al. (2010). Iodine speciation in marine aerosols along a 15000-km round-trip cruise path from Shanghai, China, to the Arctic Ocean. *Environmental Chemistry*, 7(5), 406–412. <https://doi.org/10.1071/en10048>
- Yodle, C. (2015). *Iodine speciation in marine aerosol* (Doctoral dissertation). Norwich, UK: University of East Anglia.
- Yodle, C., & Baker, A. R. (2019). Influence of collection substrate and extraction method on the speciation of soluble iodine in atmospheric aerosols. *Atmospheric Environment: X*, 1, 100009. <https://doi.org/10.1016/j.aeaoa.2019.100009>
- Yu, H., Ren, L., Huang, X., Xie, M., He, J., & Xiao, H. (2019). Iodine speciation and size distribution in ambient aerosols at a coastal new particle formation hotspot in China. *Atmospheric Chemistry and Physics*, 19(6), 4025–4039. <https://doi.org/10.5194/acp-19-4025-2019>
- Zhang, L., Hou, X., & Xu, S. (2016). Speciation of 127I and 129I in atmospheric aerosols at Risø, Denmark: Insight into sources of iodine isotopes and their species transformations. *Atmospheric Chemistry and Physics*, 16(4), 1971–1985. <https://doi.org/10.5194/acp-16-1971-2016>
- Zhou, Y., Huang, X. H., Bian, Q., Griffith, S. M., Louie, P. K. K., & Yu, J. Z. (2015). Sources and atmospheric processes impacting oxalate at a suburban coastal site in Hong Kong: Insights inferred from 1 year hourly measurements. *Journal of Geophysical Research: Atmospheres*, 120, 9772–9788. <https://doi.org/10.1002/2015JD023531>